Soft Matter

View Online
Dynamic Article Links

Cite this: *Soft Matter*, 2011, **7**, 3533

www.rsc.org/softmatter

PAPER

Relaxation dynamics in the columnar liquid crystal phase of hard platelets

Alessandro Patti,†*[a] Simone Belli,[b] René van Roij[b] and Marjolein Dijkstra[a]

Received 5th November 2010, Accepted 13th January 2011
DOI: 10.1039/c0sm01265c

We perform Monte Carlo simulations to analyze the equilibrium dynamics and the long-time structural relaxation decay of columnar liquid crystals of disk-like colloidal particles. In the wake of recent studies on the columnar mesophase of hard calamitic (rod-like) colloids, we now focus on the diffusion of their discotic counterparts, here modeled as oblate hard spherocylinders. These systems exhibit a non-Gaussian column-to-column diffusion due to the combined action of transient cages and periodic free-energy barriers. We find that at fixed packing fraction the barrier height increases with decreasing particle thickness, resulting into a more heterogeneous and non-Gaussian dynamics for thinner platelets, and reducing the inter-column diffusion coefficient. Moreover, we observe the characteristic two-step relaxation decay of the structure in the plane perpendicular to the column axis. By contrast, the in-column dynamics is similar to the typical single-file diffusion of one-dimensional dense fluids, with a relatively fast decay of the correlation functions.

1. Introduction

Although the formation of liquid crystals of discotic particles had already been predicted in the 1920s,[1] theoretically investigated since the 1950s,[2–5] and experimentally hypothesised in the 1960s,[6] the first unequivocal evidence of their existence is significantly more recent and due to Chandrasekhar and co-workers.[7] Their seminal work on the hexaesters of benzene disclosed an exciting and fascinating field in liquid crystal research, adding new potential applications to those already offered by liquid crystals of calamitic (rod-like) molecules. These authors observed a novel mesophase in which the molecules were arranged on top of each other, forming oriented stacks and determining the well-known columnar (*Col*) liquid crystal phase. The *Col* phase is generally classified by considering the stacking of the molecules inside each column, and the long-range arrangement of the two-dimensional (2D) inter-column lattice.[8–12] Depending on the in-column interactions, the mesogens can be aligned, tilted, or irregularly stacked with respect to the column axis. In any of these three cases, due to the lack of an appreciable long-range translational order, the columns are regarded as one-dimensional (1D) fluids. As far as the inter-column order is concerned, the *Col* phase can show a rectangular, oblique, or hexagonal 2D symmetry, with the columns parallel to each other. Therefore, the columnar phase behaves as a crystal in the direction of the lattice vectors.

Columnar liquid crystals of discotic platelets (CLCDs) are gaining an increasing relevance in technological applications whether their scale is tens of Angstroms (molecular scale) or hundreds of nanometres (colloidal scale). Understanding their equilibrium and out-of-equilibrium aggregation behavior is also an interesting challenge for fundamental research on stacking phenomena. The most common and frequently investigated molecular CLCDs are formed by mesogens, such as triphenylenes[13–15] or hexabenzocoronenes,[16–18] with a rather rigid central aromatic core surrounded by flexible peripheral alkyl chains bonded to the edges.[11,19] Both the core and the side chains can be tailored to control and eventually to improve the functional properties of the material.[16,20] Remarkably, the spontaneous supramolecular self-assembly in ordered columnar aggregates increases the mobility of electrons and charge carriers through the cores and along the stacked arrangements.[21,22] Due to the insulating effect of the lateral hydrocarbon chains, the interactions established between neighboring mesogens within the same column are significantly stronger than those between mesogens of contiguous columns,[23,24] and a (quasi) 1D charge transport is observed.[25–27] As a consequence of this peculiar behavior, the conducting properties of CLCDs offer the advantage to improve the performance of electronic, optoelectronic, and photovoltaic devices, such as solar cells and plastic organic field-effect transistors.[28–35] In all these applications, the liquid crystalline properties of CLCDs, and in particular their fluid-like dynamics along the columns, are of fundamental importance in the self-healing of eventual structural defects, such as grain boundaries, which might hamper the charge diffusion by trapping the charge carriers.[20,36]

[a]*Soft Condensed Matter, Debye Institute for NanoMaterials Science, Utrecht University, Princetonplein 5, 3584 CC Utrecht, The Netherlands. E-mail: a.patti@uu.nl; m.dijkstra1@uu.nl*
[b]*Institute for Theoretical Physics, Utrecht University, Leuvenlaan 4, 3584 CE Utrecht, The Netherlands. E-mail: s.belli@uu.nl; r.vanroij@uu.nl*
† Present address: Instituto de Química Avanzada de Catalunya - Centro Superior de Investigaciones Científicas, C/Jordi Girona, 18–26, 08034 Barcelona, Spain. E-mail: alessandro.patti@iqac.csic.es

On the colloidal scale, CLCDs have recently been used by Mourad *et al.* as templating agents for the synthesis of ordered macroporous silica structures.[37] Motivated by the necessity to prepare hexagonally-packed materials with larger pores than those synthesized in the 1990s with surfactants (MCM-41)[38] or block copolymers (SBA-15),[39] these authors used CLCDs of colloidal gibbsite platelets to generate ordered silica materials with pore diameters in the macroporous range (50–1000 nm), that is well above the usual pore sizes achieved with amphiphilic templates. Colloidal gibbsite platelets, which show a rich phase behavior,[40] were also used to show the formation of columnar liquid crystals in highly polydisperse systems,[41] and they are able to aggregate in nematic droplets (tactoids) under the influence of a magnetic field.[42] Laponite clay platelets have been the object of interesting discussions regarding the characterization of their aggregation state at high densities.[43–47]

For the time being, the amount of experimental research devoted to analyze the properties and improve the technological applications of CLCDs overwhelms the number of computational investigations, which have mostly focused on the behavior of platelets in the isotropic or nematic phase.[48–58] In fact, discotic mesogens are rather complex organic molecules and many of them are required to properly simulate the phase and aggregation behavior as well as the dynamics in the *Col* mesophase. Atomistic models provide a worthwhile tool to access the details of liquid crystals at the molecular level, but they are too computationally demanding to handle more than some tens of mesogens during an appropriate time interval. The first molecular dynamics simulations, published almost twenty years ago, limited their analysis to few tens of molecules and to a too short time interval (100–200 ps).[59,60] Due to the long time scales involved in the relaxation dynamics of these systems, only longer simulations can guarantee the independence of the results on the starting configurations. More recently, Cinacchi *et al.* carried out a more reliable 10 ns atomistic simulation of 80 discotic molecules to study the structure and translational dynamics of the columnar mesophase of a triphenylene.[61] Andrienko *et al.* adopted the united atom approach to simulate, for a time of 100 ns, 160 discotic molecules stacked in columns of ten molecules each, with hexagonal or rectangular arrangement as initial configurations.[62] Cristinziano and Lelj performed molecular dynamics simulations at atomistic level to study the transition from isotropic to columnar phase of a metal-porphyrazine complex.[63] They analyzed the organization of 64 mesogens in the columns with particular focus on the conformation of their side chains during the phase transition.

The prevailing perception, also underlined by the authors of Ref. 62, is that atomistic simulations cannot supply a comprehensive picture of the dynamics in the *Col* mesophase, because of the limited time and length scales they can achieve. However, their output can be of fundamental importance to improve the accuracy of the approximations made in coarse-grained (CG) models.[64] CG models, where a number of atoms are arranged together in a simplified fashion, have extensively and efficiently been used to describe the phase behavior[65–68] and the relaxation dynamics[69–72] of liquid crystals of rod-like particles. An efficient CG model for CLCDs has been proposed and developed in the last two years by Cuetos and Martínez-Haya to investigate the phase behavior of fluids of rigid discotic particles with hard or soft interactions.[73–75] Their oblate hard spherocylinder (OHSC) model overcomes the limits of the ellipsoidal and cut-sphere (CS) models in the analysis of the *Col* mesophase. More specifically, hard ellipsoids cannot self-assemble into the columnar phase[76] unless suitable soft interactions are included.[77] Hard cut spheres do form columnar liquid crystals,[78] but their application is limited by the complexity of including interactions with the same shape anisotropy as the core.[74] Furthermore, the CS model cannot predict the formation of one crystal phase observed experimentally in systems of platelets: the tilted crystal phase, where the molecular plane of the particles is tilted with respect to the column axis.[22] Recent free energy calculations demonstrated the stability of this peculiar structure in the phase diagram of the OHSC model.[79,80]

In the wake of previous studies on calamitic colloidal particles,[69–72] we now turn our attention to the relaxation dynamics of discotic particles in the columnar liquid crystal mesophase. In spite of the substantial differences in the equilibrium phase behavior between liquid crystal phases of calamitic and discotic particles, we find interesting similarities in their rattling-and-jumping diffusion and two-step relaxation dynamics. Although, a straight comparison between the present systems of monodisperse platelets and the binary mixtures of rods of Ref. 72 is not always feasible, we will identify and discuss some common features throughout this paper. To our knowledge, although understanding the dynamics of CLCDs is of fundamental and technological importance, the present contribution represents the first attempt to disclose the physics behind the long-time structural relaxation decay of CLCDs. Additionally, given that the difference between the Brownian motion of colloids and the ballistic motion of molecules at very short time scales is unimportant for their long-time dynamics, as several simulation studies pointed out,[81–83] our conclusions on the structural relaxation of hard colloidal CLCDs are still valid for their molecular counterparts. We note that the relaxation dynamics of hard platelets has recently been investigated by Bier and van Roij applying a dynamic density functional theory.[84] These authors studied the formation of dense elongated clusters of infinitely thin square cuboids under the influence of an external potential, but limited their analysis to the isotropic phase. In this paper, we investigate the heterogeneous inter-column dynamics in CLCDs of OHSCs and the associated non-Gaussian behavior due to the presence of periodic barriers and transient cages that hamper and delay the diffusion of the particles. We observe the typical characteristics of the rattling-and-hopping diffusion from a column to another, and those of single-file diffusion[85] along the same column.

2. Model and simulations

The geometrical shape of the OHSC model for discotic particles is pictured in Fig. 1. It consists of a central cylindrical body, with diameter σ and height L, surrounded by a toroidal rim with tube radius $L/2$. Therefore, the overall diameter of the OHSC is given by $D = \sigma + L$. The aspect ratio, $L^* = L/D$, is the only relevant geometric parameter which rules the phase behavior and the dynamics of these systems, along with the packing fraction $\eta = Nv_0/V$, where V is the volume of the system, N the number of

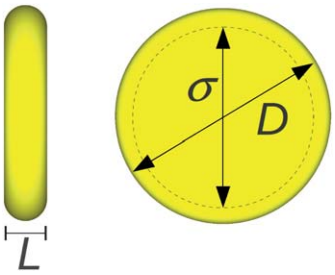

Fig. 1 Side view (left) and top view (right) of an oblate spherocylinder with diameter D and thickness L. The diameter of the cylindrical body is $\sigma \equiv D - L$.

particles, and $v_0 = \pi/6[L^{*3} + (3\pi/4)L^{*2}(1 - L^*) + (3/2)(1 - L^{*2})L^*]D^3$ their molecular volume.[86]

A preliminary study explored recently the phase behavior of systems containing OHSCs by direct MC simulations[73] and subsequently the phase diagram has been determined using free energy calculations.[79,80] The phase diagram of OHSC as obtained from free-energy calculations is shown in Fig. 2. It shows features analogous to the CS phase diagram,[78,87] with isotropic (*I*), nematic (*Nem*), columnar (*Col*), and crystal (*K*) phases. However, due to the particle shape, the CS and OHSC phase diagrams deviate from each other in some relevant aspects. In fact, OHSCs do not show a stable cubatic phase, observed for cut spheres,[78] and they may assemble in two stable crystal structures instead of one. More specifically, for $0 \leq L^* \leq 0.3$, a stable *Col* phase is observed, which transforms into a tilted crystal phase (K_t) at high pressures. The second crystal phase, K_a, is observed for $L^* > 0.45$ and consists of perfectly aligned particles. The *Col* phase melts into a *Nem* phase for aspect ratios $L^* \leq 0.1$, and into an *I* phase for $0.1 < L^* < 0.3$. For $L^* > 0.3$, the *Col* phase is not stable and the *I* phase first transforms into a K_t and, at higher aspect ratios, into a K_a phase.[79,80]

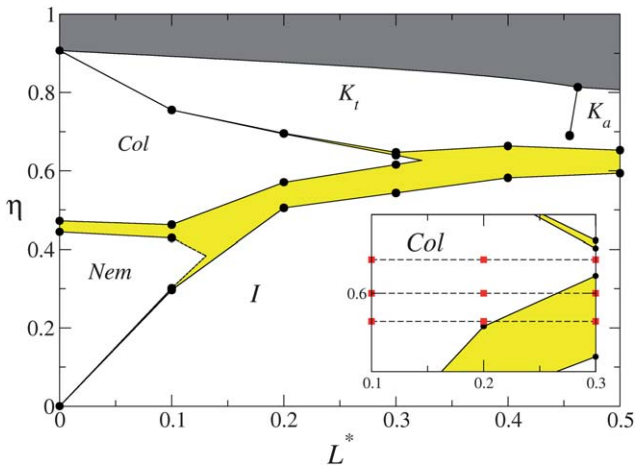

Fig. 2 Phase diagram of oblate hard spherocylinders in packing fraction (η) *versus* length-to-diameter ratio (L^*) as obtained by free-energy calculations from Ref. 79,80. *I*, *Nem*, *Col*, K_t, and K_a indicate the isotropic, nematic, columnar, tilted crystal, and aligned crystal phases, respectively. The light-shaded area denotes a two-phase coexistence region, whereas the dark-shaded area contains inaccessible state points which lie above the close packing line. In the inset, we show the nine state points studied in this paper (red squares).

The focus of the present paper is on the relaxation dynamics in the *Col* phase of OHSCs. We performed Monte Carlo (MC) simulations in a cuboidal box of volume V with periodic boundary conditions. Our systems with $L^* = 0.1$, 0.2, and 0.3 consist of $N = 3840$, 1792, and 1280 particles, respectively, to allow an integer number of columns to fit in a box of similar length along the three dimensions. To equilibrate the columnar phases, we expanded the system from an ordered crystalline phase in the constant-pressure ensemble. Each MC cycle consisted of N attempts to displace and/or rotate randomly selected particles, plus an attempt to anisotropically change the box volume at constant pressure $P^* = \beta P D^3$, with $\beta = 1/k_B T$, k_B the Boltzmann constant and T the temperature. As usually, translational and rotational moves were accepted if no overlap was detected. The overlap check is based on the computation of the distance between OHSCs, which implies to estimate the distance between two-dimensional flat disks. This mathematical problem has been addressed by several authors in the last three decades.[73,86,88,89] Here, we apply the algorithm proposed by Cuetos and Martínez-Haya, which extends those proposed by Wojcik and Gubbins,[86] and later by Almohamad and Selim.[89] We refer the interested reader to the Appendix of Ref. 73 for technical details.

The systems were considered at equilibrium when the packing fraction achieved a steady value within the statistical fluctuations. The equilibrated configurations were used to examine the relaxation dynamics by performing MC simulations in the isochoric-isothermal (*NVT*) ensemble. The volume was kept constant to prevent unphysical collective moves which would not reproduce rigorously the stochastic Brownian motion of the particles. In this case, one MC cycle, which we set as unit of time, only consisted of N attempts to displace and/or rotate particles. Time scales can be easily converted in units of the short-time diffusion coefficients which we will calculate below for the systems of interest. It is worth noting that the short-time diffusion coefficients for micron-sized colloidal disks is $D_S \sim 1$ μm^2/s and for molecular discotic mesogens $D_S \sim 100$ μm^2/s. The time scale, that we probe here, corresponding to 10^7 MC cycles, is of the order of 10^{-1} s for colloidal disks and 10 s for molecular discotic platelets. Moreover, due to the relevant density of the columnar mesophases studied here, we can safely neglect the contribution of hydrodynamics with respect to the excluded volume interactions, as observed in colloidal suspensions of rod-like particles.[90]

Standard MC simulations have been applied to mimic the rattling-and-jumping diffusion of prolate hard spherocylinders (PHSCs) in smectic[69–71] and columnar[72] liquid crystal phases. Moreover, they were shown to be very efficient to investigate the slow relaxation dynamics in glasses.[91,92] In all these studies, the average length scale of elementary moves is determined by fixing the maximum step size, δR_{max}. This is usually chosen according to (*i*) a reasonable CPU time per simulation run, (*ii*) a satisfying acceptance rate, and (*iii*) an adequate description of the Brownian motion of colloidal particles suspended in a fluid. However, although the short-time dynamics could be missed if δR_{max} is chosen too big, any reasonable and convenient choice of δR_{max} should not affect the dynamics at long time scales. We checked that, apart from an overall scaling of the time-lengths, this was indeed the case. In systems of anisotropic particles,

where the shape has a direct effect on the short-time diffusion, δR_{max} is better decoupled into two terms: $\delta R_{max}^{\perp}$and $\delta R_{max}^{\parallel}$, which refer to the inter-column and in-column displacements, respectively. The ratio between these two terms must satisfy the following relation:

$$\frac{\delta R_{max}^{\perp}}{\delta R_{max}^{\parallel}} = \sqrt{\frac{D_S^{\perp}}{D_S^{\parallel}}}, \tag{1}$$

where $D_S^{\perp}$ and $D_S^{\parallel}$ are the short-time diffusion coefficients of the OHSC in the direction perpendicular and parallel to its short axis, respectively. To our knowledge, there are no available expressions for the self-diffusion coefficients of OHSCs. Therefore, we make use of the analytical expressions proposed for oblate ellipsoids,[93,94] which were more recently applied to investigate the Brownian dynamics of colloidal suspensions of Laponite clay platelets.[95] We argue that possible deviations given by the difference in shape of the two discotic particles are negligible, such that the ratio between the short-time diffusion coefficients reads[95]:

$$\frac{D_S^{\perp}}{D_S^{\parallel}} = \frac{1}{2}\frac{(3\nu^2-2)\lambda - 1}{(\nu^2-2)\lambda + 1}, \tag{2}$$

where $\nu = 1/L^*$ and $\lambda = \left(\nu^2-1\right)^{-1/2}\arctan\left(\sqrt{\nu^2-1}\right)$. The relative values of the self-diffusion coefficients and maximum step sizes are given in Table 1.

The ratio between the short-time rotational diffusion coefficients, computed by applying similar analytical expressions as those of eqn (2),[95] is ~1 regardless of the particle aspect ratio. As a consequence, the maximum elementary rotation around the short axis and that around the direction perpendicular to it can be assumed to be of the same magnitude, that is $\delta\phi_{max}^{\parallel} \simeq \delta\phi_{max}^{\perp} \equiv \delta\phi_{max}$. We simultaneously fixed δR_{max} and $\delta\phi_{max}$ to yield an acceptance rate of ~50% per translational and rotational move, respectively.

In order to describe the inter-column diffusion and the long-time structural relaxation of the columnar phase of OHSCs, we computed (*i*) the transverse free-energy barrier, (*ii*) the self part of the van Hove correlation function (s-VHF), (*iii*) the non-Gaussian parameter (NGP), (*iv*) the mean square displacement (MSD), and (*v*) the self part of the intermediate scattering function (ISF).

Transverse free-energy barrier

We computed the free-energy barriers from the (relative) probability $\pi(x,y)$ of finding a particle at a given position (x,y) in the direction perpendicular to the director **n**. This probability is proportional to the Boltzmann factor, as defined in Ref. 96:

$$\pi(x,y) \propto \exp\left[-\frac{U(x,y)}{k_B T}\right], \tag{3}$$

where $U(x,y)$ denotes the effective potential for the inter-column diffusion and the proportionality constant is fixed in such a way that the minima of the potential are set to zero.

Self-part of the van Hove correlation function

To describe the inter-column rattling-and-jumping diffusion of the OHSCs, we compute the s-VHF.[97] This correlation function measures the probability distribution for a particle displacement **r** after an interval of time t. We separately estimate the s-VHF along **n** and in the plane perpendicular to **n** by evaluating the functions:

$$G_s^{\parallel}(z,t) = \frac{1}{N}\left\langle \sum_{j=1}^{N} \delta\left(z - z_j(t+t_0) + z_j(t_0)\right)\right\rangle \tag{4}$$

$$G_s^{\perp}(r_{\perp},t) = \frac{1}{N}\left\langle \sum_{j=1}^{N} \delta\left(r_{\perp} - r_{\perp,j}(t+t_0) + r_{\perp,j}(t_0)\right)\right\rangle_{2\pi}, \tag{5}$$

with $(r_{\perp,j}(t),z_j(t))$ the location of particle j at time t, δ the Dirac-delta, $\langle\cdots\rangle$ the ensemble average. The index 2π indicates the average over the polar angle which defines the bidimensional vector $r_{\perp}$. It should be noticed that for freely diffusive particles these functions are described by a Gaussian.

Non-Gaussian parameter

The NGP gives a quantitative description of the deviations from Gaussian behavior. It is defined as[98]

$$\alpha_2(t) = \frac{\left\langle \mathbf{r}^4(t)\right\rangle}{(1+2/d)\left\langle \mathbf{r}^2(t)\right\rangle^2} - 1 \tag{6}$$

Table 1 Details of the systems that we studied in this paper, consisting of oblate hard spherocylinders with varying length-to-diameter ratios $L^* = L/D$, reduced pressures $P^* = \beta P D^3$, and corresponding packing fractions η. For comparison, we give the nematic order parameter S_{nem}, the ratio of the self-diffusion coefficients, $D_S^{\perp}/D_S^{\parallel}$, calculated from eqn (2), and that of the maximum displacements, $\delta R_{max}^{\perp}/\delta R_{max}^{\parallel}$; the short-time in-column diffusion coefficients, $D_S^{\parallel}$, in units of τ/D^2, with τ the time unit; the geometric parameter λ (see text and eqn (2)); the long-time inter-column, $D_L^{\perp}$, and in-column, $D_L^{\parallel}$, diffusion coefficients in units of τ/D^2; and the height of the free-energy barriers (U_0) in units of $k_B T$

L^*	0.100			0.200			0.300		
λ	0.148			0.280			0.398		
$D_S^{\perp}/D_S^{\parallel}$ (from eqn (2))	1.391			1.307			1.239		
$\delta R_{max}^{\perp}/\delta R_{max}^{\parallel}$	1.179			1.143			1.111		
$(D_S^{\parallel}\tau/D^2) \times 10^6$	3.062			6.239			9.100		
P^*	104.5	112.5	125.0	59.0	65.0	80.0	46.0	50.0	60.0
η	0.575	0.600	0.630	0.575	0.600	0.630	0.575	0.600	0.630
S_{nem}	0.96	0.97	0.98	0.92	0.94	0.95	0.85	0.90	0.91
$(D_L^{\perp}\tau/D^2) \times 10^8$	—	—	—	0.586	—	—	1.988	0.071	—
$(D_L^{\parallel}\tau/D^2) \times 10^7$	0.385	0.152	0.128	1.634	1.429	0.847	4.126	3.308	1.310
$U_0/k_B T$	12.5	19.0	27.0	9.0	13.0	25.0	8.5	12.5	17.5

where $d = 1$ for the longitudinal diffusion along **n** and $d = 2$ for the planar transverse diffusion. Heterogeneous dynamics occurs on a time scale t, if the NGP deviates from zero.

Self part of the intermediate scattering function

We examine the structural relaxation decay of the density fluctuations by measuring the self-part of the ISF,

$$F_s(q,t) = \frac{1}{N}\left\langle \sum_{j=1}^{N} \exp\left[iq\cdot\left(\mathbf{r}_j(t+t_0) - \mathbf{r}_j(t_0)\right)\right]\right\rangle, \qquad (7)$$

at the wave vectors $(q_x^*,q_y^*,0)$ and $(0,0,q_z^*)$, which correspond, respectively, to the first peak of the structure factor in the perpendicular and parallel directions to **n**. In particular, the transverse and longitudinal relaxations will be given by $F_s^{\perp}(t) = F_s((q_x^*,q_y^*,0),t)$ and $F_s^{\parallel}(t) = F_s((0,0,q_z^*),t)$, respectively.

3. Results

We studied 9 state points of OHSC systems, characterized by the three packing fractions $\eta = 0.575$, 0.600, and 0.630, for the aspect ratios $L^* = 0.1$, 0.2, and 0.3. In Fig. 3, we show equilibrium configurations of CLCDs with $L^* = 0.1$ (*a*, *b*), 0.2 (*c*, *d*), and 0.3 (*e*, *f*), all at $\eta = 0.575$. By visual inspection, it appears evident that the in-column order is higher for the most aspherical particles, with $L^* = 0.1$, which are significantly more aligned than those with $L^* = 0.2$ or 0.3. For $L^* = 0.3$, we even find small clusters of particles with orientations perpendicular to the nematic director **n**, which is oriented along the longitudinal direction z. This is confirmed by the computation of the nematic order parameter defined by the second Legendre polynomial: $S_{nem} = \langle 3(\mathbf{u}_i\cdot\mathbf{n})^2 - 1\rangle/2$, where u_i is the individual orientation of a particle. S_{nem} quantifies the longitudinal order of the discotic particles, regardless of the 2D symmetry of the hexagonal lattice. Therefore, it can be regarded as an in-column order parameter. At $\eta = 0.575$, S_{nem} is equal to 0.96, 0.92, and 0.85, for $L^* = 0.1$, 0.2, and 0.3, respectively. An analogous tendency is also observed at higher packing fractions (see Table 1). The gradual loss of in-column alignment with increasing L^* is a consequence of the phase behavior of the OHSC model (see Fig. 2). At $L^* = 0.1$ and $\eta = 0.575$, the system is well-inside its stable *Col* phase, far from *Nem*-*Col* phase coexistence with the *Nem* phase, which is located at $\eta \simeq 0.45$. By contrast, the systems containing particles with $L^* = 0.2$ and 0.3, at the same packing fraction, are just above the *I*-*Col* phase coexistence region or unfortunately inside the two-phase region. At the time we started the simulations, the *I*-*Col* phase boundaries were not known. This relevant distinction plays a crucial role in the inter-column diffusion of the particles, as we will discuss below. For comparison, it is interesting to note that in smectic liquid crystals, freely-rotating hard rods diffuse from a layer to another easier than perfectly aligned hard rods, as observed in Ref. 71.

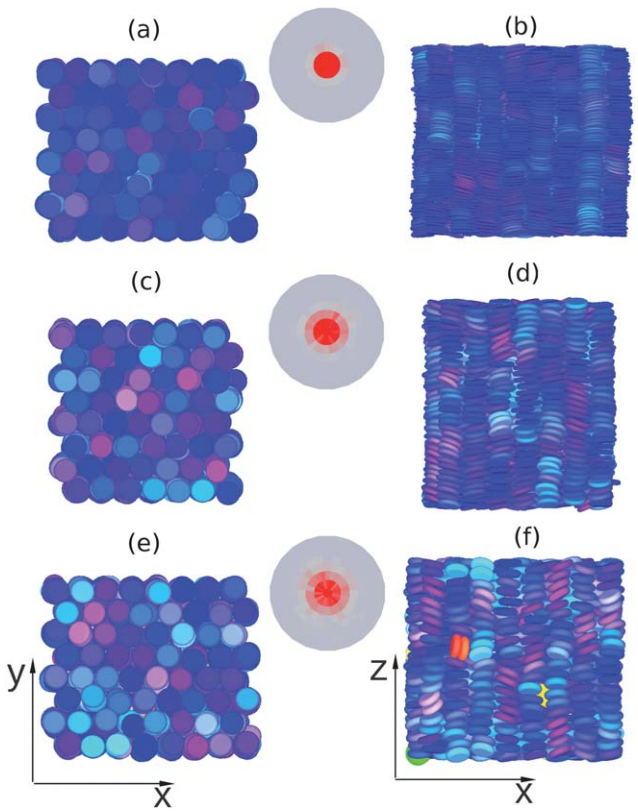

Fig. 3 Top (left) and front (right) views of the columnar phase of oblate hard spherocylinders with $L^* = 0.1$ (a, b), $L^* = 0.2$ (c, d), and $L^* = 0.3$ (e, f), at $\eta = 0.575$. The gray spheres in the middle show the orientational distribution of the molecular short axes. The particles assume different colors according to their orientation.

The structural order of CLCDs can be better appreciated by computing the pair correlation functions along the director **n** and in the plane perpendicular to it. In Fig. 4 and 5, we give, respectively, the transverse, $g_{\perp}(r_{\perp})$, and the longitudinal, $g_{\parallel}(z)$, pair correlation functions for the nine systems of interest. The inter-column order is neither particularly affected by the shape anisotropy nor by the packing of the system (see Fig. 4(a, b, c)). In fact, the location of the peaks of $g_{\perp}$ follows the hexagonal arrangement of the particles in the 2D lattice, with a gradual shifting towards lower $r_{\perp} = \sqrt{x^2 + y^2}$ with increasing density, and it is similar for the three aspect ratios (see also Ref. 73). On the other hand, the in-column pair correlation functions, $g_{\parallel}$, present distinctive features which are coherently linked to the alignment of the particles into the columns, as detected in Fig. 3. More specifically, we note periodically peaked positional correlations which persist to long distances and decay slowly to unity for the denser systems. By contrast, at lower packing fractions, the correlation length is shorter and $g_{\parallel}$ decays faster to one. Long-range spatial correlations were previously observed by MC simulations for aspect ratios $0.2 \leq L^* \leq 0.5$,[73] where the authors distinguished between interdigitated (D_{hi}), ordered (D_{ho}), and disordered (D_{ho}) columnar phases, depending on the inter- and in-column alignment of particles. Free-energy calculations showed that the D_{hi} phase is actually a K_t or a K_a phase with many defects.[79] In agreement with the latter results, which set the *Col*-K_t transition at η>0.7, we did not determine any sign of interdigitation at $L^* = 0.1$ and 0.2 for the densities studied here. In fact, the $g_{\parallel}$ in Fig. 5(a) and 5(b) show peaks at approximately integer multiples of the particle thickness L^*. At $L^* = 0.3$, the development of a second peak in Fig. 5(c) at approximately integer multiples of $L^*/2$, which is limited to a relatively short correlation length, suggests that our systems are very close to the K_t phase transition, again in agreement with Ref. 79,80.

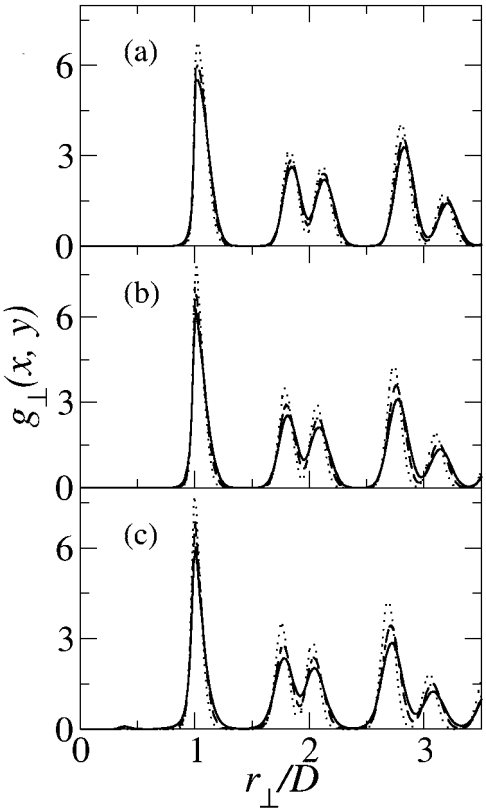

Fig. 4 Transverse pair-correlation function, $g_\perp(r_\perp)$, as a function of $r_\perp = \sqrt{x^2 + y^2}$, in columnar liquid crystals of oblate hard spherocylinders with length-to-diameter ratios $L^* = 0.1$ (a), $L^* = 0.2$(b), and $L^* = 0.3$ (c). The solid, dashed, and dotted lines refer to the packing fractions $\eta = 0.575$, 0.600, and 0.630, respectively.

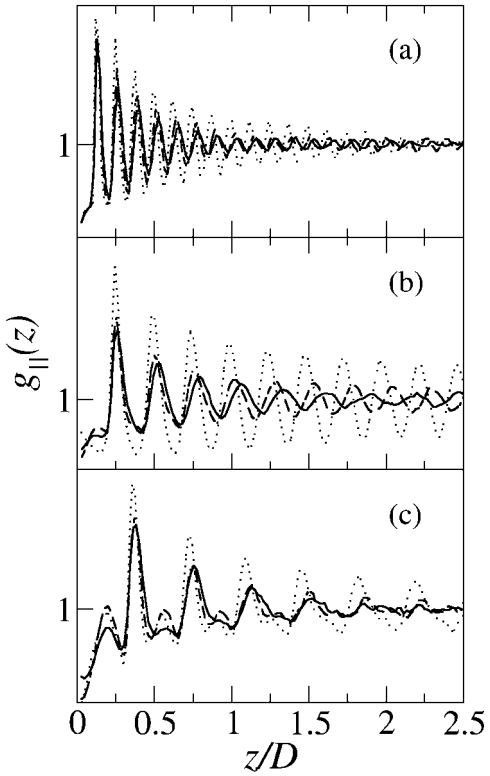

Fig. 5 Longitudinal pair-correlation function, $g_\parallel(z)$, as a function of z, in columnar liquid crystals of oblate hard spherocylinders with length-to-diameter ratios $L^* = 0.1$ (a), $L^* = 0.2$(b), and $L^* = 0.3$ (c). The solid, dashed, and dotted lines refer to the packing fractions $\eta = 0.575$, 0.600, and 0.630, respectively.

The 2D hexagonally packed arrangement of the columns yields an effective periodic potential $U(x,y)$ for the diffusion of discotic particles from a column to another. This effective potential, introduced in eqn (3), quantifies the effect of permanent free-energy barriers on the inter-column diffusion, similarly to what has recently been observed in experiments [96] and simulations[69–72] of columnar and smectic liquid crystals. In all these studies, it was found that to diffuse along the broken 1D (smectic) or 2D (columnar) symmetry direction, a particle must overcome a free-energy barrier of the order of a few k_BT, depending mostly on the packing of the system, but also on the particle anisotropy and on the rotational degrees of freedom. In Fig. 6, we give a 2D representation of the mean-field effective potential throughout the transverse direction to the director **n**. The blue regions, which overlap with the 2D lattice positions, denote the minima of the potential, and hence the peak in the density distribution of the particles. By contrast, the reddish areas, located in between neighboring columns, indicate the maxima of the potential, *i.e.* the unfavorable locations for the particles. To give an estimate of the height of the barrier as a function of density and aspect ratio, we show in Fig. 7 a transverse section of the free-energy landscapes obtained from Fig. 6 and fit the points with the following sinusoidal function:

$$U(x,y) = \sum_{k=1}^{m} U_k \left(\sin \frac{\pi r_\perp}{h} \right)^{2k} \qquad (8)$$

where m is an integer cut-off, and U_k and h fitting parameters. As a general tendency, the height of the free-energy barriers increases from $\eta = 0.575$ to $\eta = 0.630$ for the three anisotropies studied here. The particles in the denser state are then much more confined in the original columns, and their diffusion to other columns is strongly inhibited. This is especially evident at $L^* = 0.2$ and 0.3 as the peak of the barrier increases from $\sim 8k_BT$ to the significantly high value of $\sim 25k_BT$ that basically prevents the inter-column diffusion. Furthermore, we note that at constant packing fraction, increasing the anisotropy leads to higher free-energy barriers. At $\eta = 0.600$, for instance, the barrier height is $11k_BT$, $15k_BT$, and $19k_BT$, at $L^* = 0.3$, 0.2, and 0.1, respectively. We conclude that, as observed in columnar mesophases of calamitic particles,[72] both packing and anisotropy have a remarkable impact on the height of the free-energy barriers.

The inter-column free-energy barriers shed light on the effect of the transverse hexagonal symmetry of the *Col* phase on the diffusion of the discotic particles. More specifically, their periodic shape provokes and characterizes the rattling-and-jumping motion of the particles in the 2D lattice. To better appreciate the effect of the combined action of permanent barriers and temporary cages on the long-time diffusion, we exemplarily show in Fig. 8 the planar displacements of $N = 1280$ particles with $L^* = 0.3$ collected at $\eta = 0.575$ from $t^* \equiv t/\tau = 10$ to $t^* = 10^7$, with τ the time unit. At $t^* = 10$, the platelets are still very close to their original position, rattling in the cage formed by the surrounding neighbors. At longer times, they have crossed

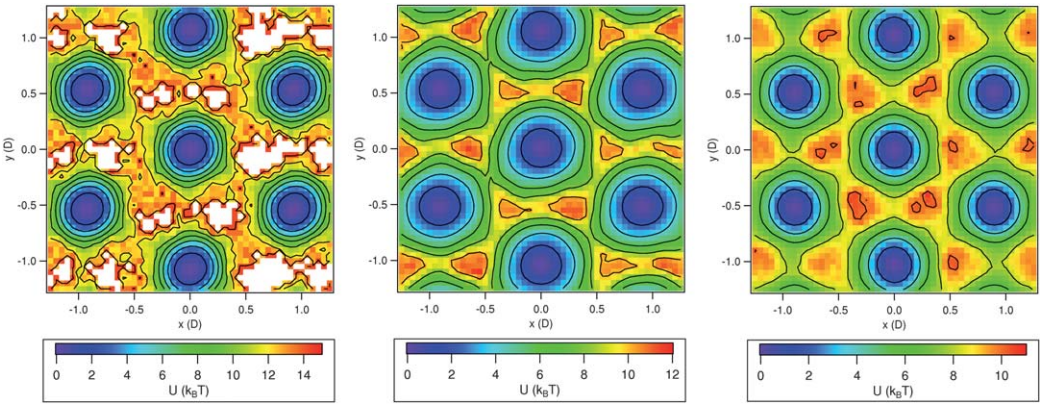

Fig. 6 Mean-field effective potential $U(x,y)$ in units of k_BT for the column-to-column diffusion in systems of oblate hard spherocylinders with length-to-diameter ratios $L^* = 0.1$, 0.2, and 0.3, from left to right, respectively. The packing fraction is $\eta = 0.575$ for the three systems. The black isopotential lines represent the points in which the potential is equal to a multiple of $2k_BT$, from $2k_BT$ to $14k_BT$.

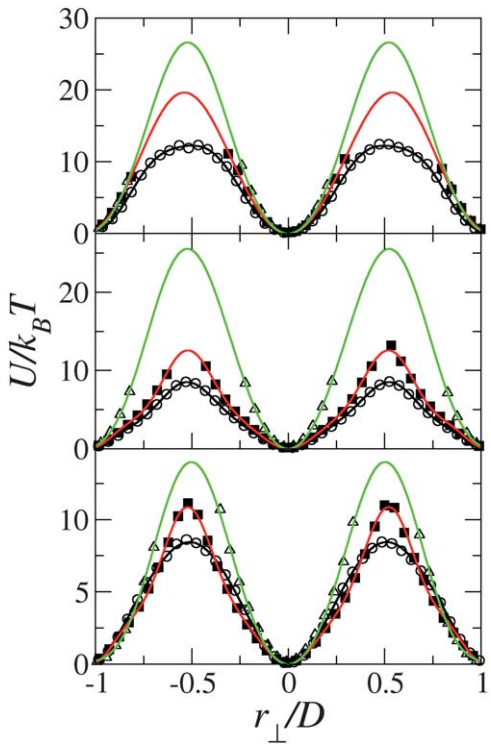

Fig. 7 Transverse section of the mean-field effective potential $U(x,y)$ in Fig. 6 for the column-to-column diffusion in columnar liquid crystals of hard oblate spherocylinders with varying length-to-diameter ratios L^* and packing fraction η. From top to bottom: $L^* = 0.1$, 0.2, and 0.3. Circles, squares, and triangles refer to $\eta = 0.575$, 0.600, and 0.630, respectively. The solid lines are fits with $m = 5$ harmonic modes (see eqn (8)).

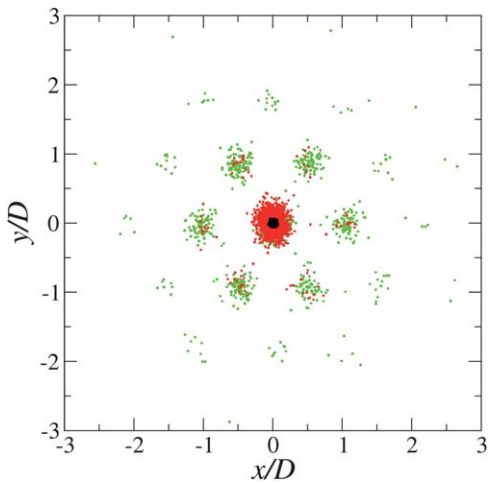

Fig. 8 Particle displacements in the planes perpendicular to the nematic director of $N = 1280$ oblate hard spherocylinders with length-to-diameter ratio $L^* = 0.3$ at $\eta = 0.575$ in the columnar phase, collected at $t^* = 10$ (black points), $t^* = 10^6$(red), and $t^* = 10^7$ (green).

the cage, overcome the barrier and finally, following the hexagonal 2D symmetry, jumped to one (at $t^* = 10^6$) or more (at $t^* \geq 10^7$) diameter distances away.

To quantify this discretized rattling-and-jumping diffusion, which suggests close analogies with the diffusion of hard rods in smectic[70] or columnar[72] liquid crystals, we compute the s-VHFs, defined in eqn (5). In Fig. 9 and 10, we present the longitudinal and transverse components of the s-VHF at several time decades for different particle anisotropies at $\eta = 0.575$ and 0.600. The s-VHF along the director **n** is in line with our previous results on columnar mesophases of rod-like particles,[72] where small deviations from Gaussianity at short time scales indicate the presence of particles able to displace rather longer distances than expected by assuming a Gaussian distribution. This behavior, which resembles that of the heterogeneous dynamics in out-of-equilibrium systems, such as supercooled liquids and gels, is a consequence of the simultaneous presence of *slow* and *fast* particles, and hence of the trapping action of the cage formed by their surrounding neighbors. However, the weight of the two sets of particles on the longitudinal dynamics of the system is limited to a relatively short time interval, and it cancels out at long time scales where the agreement with the Gaussian fits is excellent. The longitudinal dynamics of OHSCs significantly diverges from the behavior in the transverse directions, as we can appreciate in Fig. 10. In fact, the inter-column s-VHFs are not monotonic, but periodically peaked functions of $r_\perp$, and hence deviate significantly from Gaussianity. The peaks, located at quasi-quantized distances of neighboring columns, indicate that a number of

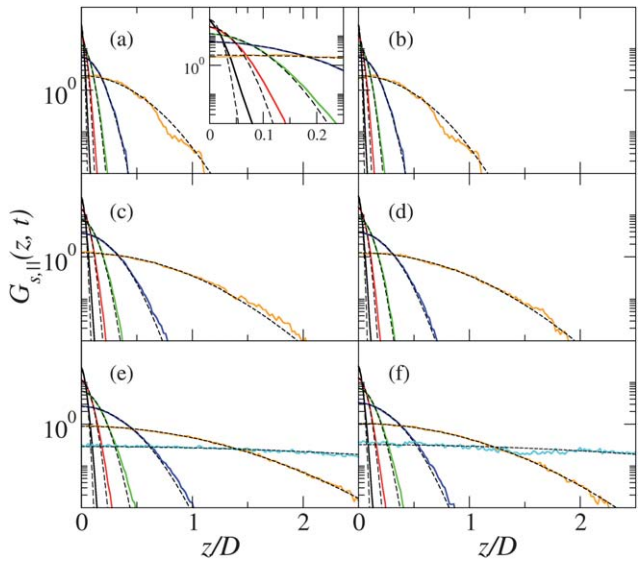

Fig. 9 Longitudinal component of the self-part of the van Hove function, $G_{s,\parallel}(z,t)$, of columnar liquid crystals of OHSCs with length-to-diameter ratios $L^* = 0.1$ (a, b), $L^* = 0.2$ (c, d), and $L^* = 0.3$ (e, f), as a function of z. The packing fractions are $\eta = 0.575$ (left column) and $\eta = 0.600$ (right column). The black, red, green, blue, and orange solid curves refer to the time scales $t^* = 10^3$, 10^4, 10^5, 10^6, and 10^7, respectively. The dashed lines are Gaussian fits. At $L^* = 0.1$ and $\eta = 0.575$, we zoom in on shorter distances to better appreciate the deviations from Gaussianity (see inset).

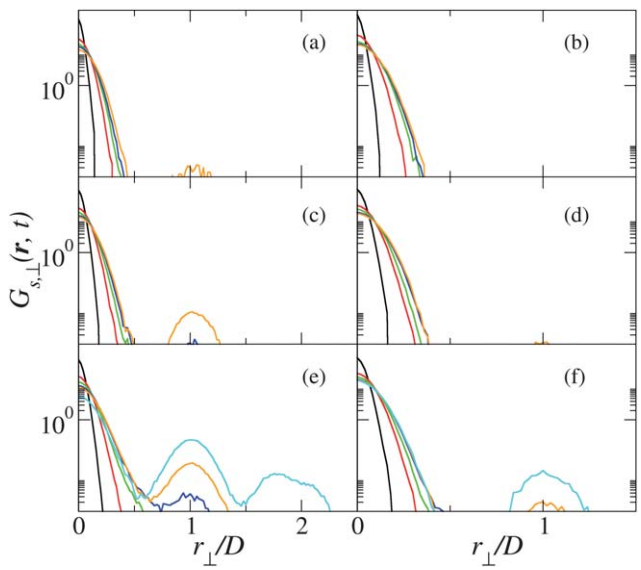

Fig. 10 Transverse component of the self-part of the van Hove function, eqn (5), of columnar liquid crystals of OHSCs with length-to-diameter ratios $L^* = 0.1$ (a, b), $L^* = 0.2$ (c, d), and $L^* = 0.3$ (e, f), as a function of $r_\perp = \sqrt{x^2 + y^2}$. The packing fractions are $\eta = 0.575$ (left column) and $\eta = 0.600$ (right column). The black, red, green, blue, orange, and cyan solid curves refer to the time scales $t^* = 10^2$, 10^3, 10^4, 10^5, 10^6, and 10^7, respectively.

fast-moving OHSCs have displaced a rather long distance even at relatively short time scales, whereas the others are still rattling around their original position. The presence of fast and slow particles determines the heterogeneous dynamics of the system and affect its long-time structural relaxation decay. We note that the height of the peaks and their number increase with decreasing pressure and increasing particles anisotropy. This is due to the distinct phase behavior of the three systems at identical packing fraction, but different anisotropy, and, more specifically, to the proximity of the *I-Col* phase coexistence. As a matter of fact, at $\eta = 0.575$ fast particles with $L^* = 0.3$ have already diffused from one to another column at $t^* = 10^5$, whereas at $\eta = 0.600$ this has only taken place at $t^* = 10^6$. It also takes one more decade of time if the anisotropy is increased to $L^* = 0.1$, at $\eta = 0.575$ (Fig. 10(a)). At $\eta = 0.630$, for any aspect ratio, the inter-column diffusion is strongly inhibited, and the profiles of the s-VHFs (not shown here) are similar to those of Fig. 10(b, d). In these cases, deviations from Gaussianity are negligible, as the analysis of the NGPs will show later on. Similar results have been recently observed in simulations,[70,72] theory,[99] and experiments[96] on smectic and columnar phases of rods. Additionally, in simulations on the layer-to-layer diffusion of rods in smectics, it was shown that the fast particles can form string-like clusters which exhibit collective motion.[69,70] We believe that in CLCDs a similar intriguing scenario might also take place, but a more detailed analysis on the particle scale is needed to clarify this aspect in detail.

Deviations from the Gaussian behavior of the VHFs in liquid crystalline systems have been analyzed by simulations,[69–72] experiments,[96] and theory[99] in terms of the non-Gaussian parameter, $\alpha_2(t)$, defined in eqn (6). The NGPs as measured in our systems are shown in Fig. 11 and 12 for the longitudinal and transverse motion, respectively. Due to the fluid-like in-column behavior, the longitudinal NGPs, $\alpha_{2,z}$, are essentially negligible for the whole time range, regardless of the system density or the particle anisotropy. By contrast, the transverse NGP, $\alpha_{2,xy}$, is characterized by two possible scenarios: it may exhibit either a time-independent behavior as a consequence of the extremely high permanent barriers which prohibit the diffusion from column to column, or a time-dependent behavior due to the transient cage effect of the surrounding particles. In the former case, the transverse dynamics of the particles is limited to the space available between adjacent columns, around their original positions. Due to this uniformly distributed behavior, $\alpha_{2,xy}$ is constantly zero. We note that, although this result is the same as that observed for $\alpha_{2,z}$, the physical interpretation on the particle scale of this macroscopic observation is rather different in the two cases. While $\alpha_{2,z}$ is zero because of the absence of permanent barriers and a relatively weak cage effect, $\alpha_{2,xy}$ is zero because of significantly high free-energy barriers which practically block the particles in their cage. In the two cases, all the particles behave homogeneously and both xy-NGP and z-NGP are identically zero. If the permanent barriers are smaller, the transverse NGPs may exhibit a time-dependent behavior due to the transient cage effect of the surrounding particles. More specifically, $\alpha_{2,xy}$ is basically zero for $t^* < 10^3$, when the disks are still rattling around their original position. For time scales in the range $10^3 < t^* < 10^4$, $\alpha_{2,xy}$ starts to deviate from zero as a consequence of the variegated dynamical behavior of the particles which can either escape their cage and diffuse to a neighboring column, or keep on rattling around the same position. Jumping from a column to another may take a relatively long time interval, during which the motion of the discotic particles becomes sub-diffusive. The deviations from Gaussian behavior increase up to $\alpha_{2,xy}^{max}$, the peak

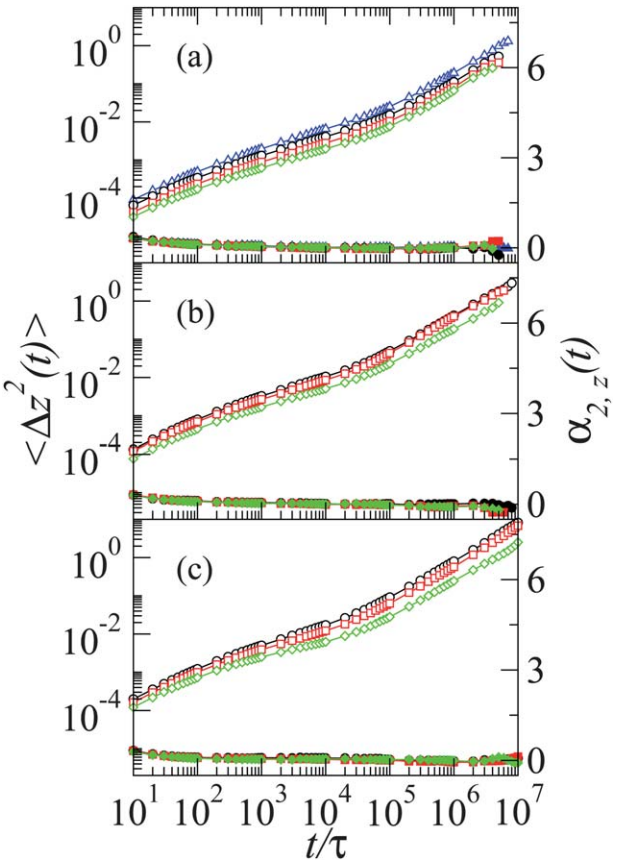

Fig. 11 Mean square displacement (open symbols), in units of D^2, and non-Gaussian parameter (solid symbols) along the nematic director, for systems of oblate hard spherocylinders with length-to-diameter ratios $L^* = 0.1$ (a), $L^* = 0.2$ (b), and $L^* = 0.3$ (c). Circles, squares, and diamonds refer to packing fractions $\eta = 0.575$, 0.600, and 0.630, respectively. For comparison, also the results at $L^* = 0.1$ and $\eta = 0.500$ are shown (triangles). Note that the vertical axes of MSDs and NGPs are on the left and right, respectively.

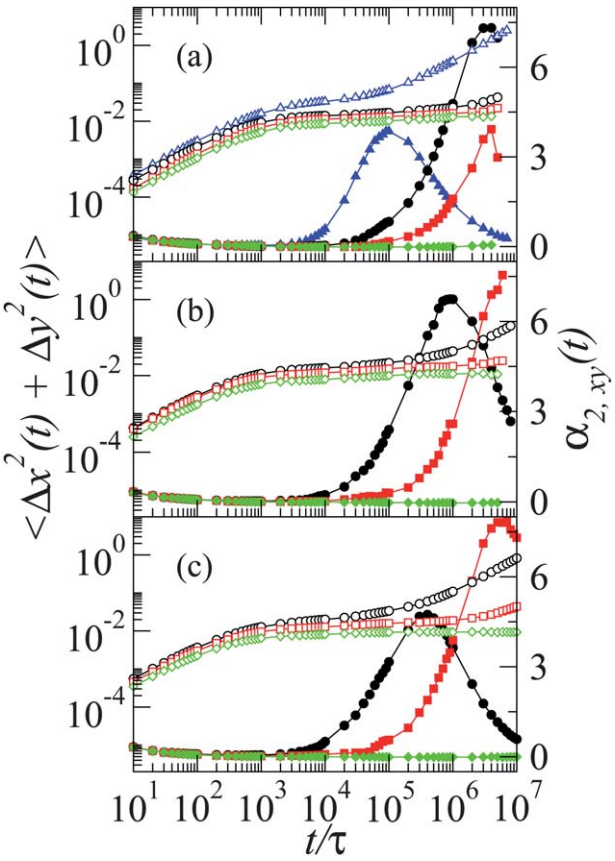

Fig. 12 Mean square displacement (open symbols), in units of D^2, and non-Gaussian parameter (solid symbols) in the plane perpendicular to the nematic director, for systems of oblate hard spherocylinders with length-to-diameter ratios $L^* = 0.1$ (a), $L^* = 0.2$ (b), and $L^* = 0.3$ (c). Circles, squares, and diamonds refer to packing fractions $\eta = 0.575$, 0.600, and 0.630, respectively. For comparison, also the results at $L^* = 0.1$ and $\eta = 0.500$ (long-time diffusion coefficient $D_L^{\perp}\tau/D^2 = 8.425 \times 10^{-8}$) are shown (triangles). Note that the vertical axes of MSDs and NGPs are on the left and right, respectively.

of the NGP, which is located at $10^5 < t^* < 10^7$, depending on the system, and determines the beginning of the long-time diffusive regime. From this time on, $\alpha_{2,xy}$ starts to decrease monotonically to zero indicating the end of the caging effect on most of the particles, which already jumped away to a different column. For the same anisotropy, we note that the peak increases with the density of the system. This phenomenon is explained by considering that a given particle can escape the trapping cage as a consequence of the rearrangement of its neighbors, which is significantly slower at higher densities as more particles are involved. Furthermore, comparison of the three systems at $\eta =$ 0.575 and 0.600, shows that the degree of non-Gaussianity and the average life-time of the caging regime, namely the height and position of $\alpha_{2,xy}^{max}$, respectively, increase for the system containing thinner platelets and higher free-energy barriers. This means that, as already found in smectic liquid crystals of calamitic particles,[70] increasing the particle anisotropy yields higher free-energy barriers and more heterogeneous and non-Gaussian dynamics.

In Fig. 11 and 12, we also plot the longitudinal and transverse mean square displacements (MSDs), $\langle\Delta z^2(t)\rangle$ and $\langle\Delta x^2(t) + \Delta y^2(t)\rangle$, respectively. As a general tendency, the xy-MSD exceeds the z-MSD only at short time scales because of the anisotropy of the short-time diffusion coefficients.[93,94] The z-MSD undergoes a rather smooth crossover from the short- to long-time diffusive regimes, as typically observed in dense fluids. This slight and relatively fast change of slope is coherent with the profiles of the longitudinal s-VHFs shown on Fig. 9, which slightly deviate from Gaussianity at low-to-moderate time scales. By contrast, the xy-MSD is characterized by three clearly distinct time dependences. The short-time dynamics, with the particles still rattling in their cage, is diffusive, that is $\langle\Delta x^2(t) + \Delta y^2(t)\rangle \propto t$. At $10^2 < t^* < 10^3$, we detect the formation of a relatively long plateau which at moderate densities extends up to t_{max}, the time at which the xy-NGP reaches the maximum, or, at higher packing fractions, may extend well beyond our simulation times. The plateau quantifies the time to escape from the trapping cages and characterizes the sub-diffusive behavior of the systems. At t_{max}, the xy-MSD becomes linear with time and the long-time diffusive regime is reached. At the highest packing fraction, $\eta = 0.630$, the free-energy barriers become so high that the sub-diffusive behavior extends well beyond our simulation time. Additionally, comparison of the MSDs for different length-to-diameter ratios

shows that, at the same packing fraction, the thicker particles diffuse faster than the others. This result is consistent with the height of the free-energy barriers of Fig. 7 and is due to the in-column arrangement of the particles, which are significantly more aligned in systems with $L^* = 0.1$. From the MSDs in the diffusive regime, we computed the longitudinal, $D_L^{\parallel}$, and transverse, $D_L^{\perp}$, long-time diffusion coefficients by applying the well-known Einstein relation along **n** and in the direction perpendicular to it, respectively:[100]

$$\frac{\partial\left\langle \Delta z^2(t)\right\rangle}{\partial t} = 2D_L^{\parallel} \tag{9}$$

and

$$\frac{\partial\left\langle \Delta x^2(t) + \Delta y^2(t)\right\rangle}{\partial t} = 4D_L^{\perp}. \tag{10}$$

We give the values of the long-time diffusion coefficients in Table 1 in units of D^2/τ, allowing a conversion from MC cycles into a more physical time unit, i. e. in units of D^2/D_L. The dynamics of each system is characterized by a diffusion coefficient in the z direction that decreases with increasing packing fraction and particle anisotropy. In the xy direction, at the highest packing fractions the diffusion is strongly inhibited and no diffusion coefficients are available. In the other cases, we observe that $D_L^{\parallel}$ is significantly larger than $D_L^{\perp}$ as a consequence of the simultaneous action of permanent barriers and temporary cages.

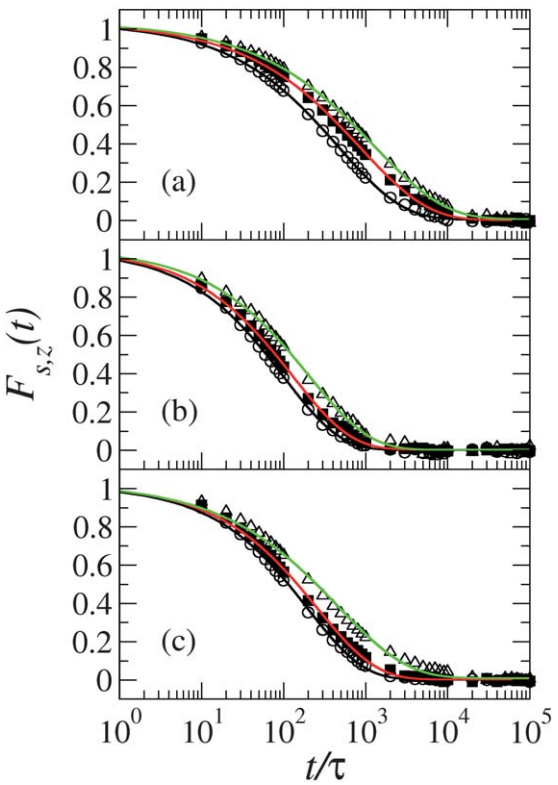

Fig. 13 Longitudinal self intermediate scattering functions, $F_{s,z}(t)$, for systems of oblate hard spherocylinders with length-to-diameter ratios $L^* = 0.1$ (a), $L^* = 0.2$ (b), and $L^* = 0.3$ (c), evaluated at packing fractions $\eta = 0.575$ (circles), $\eta = 0.600$ (squares), and $\eta = 0.630$ (triangles). The black, red, and green solid lines are fits (see text).

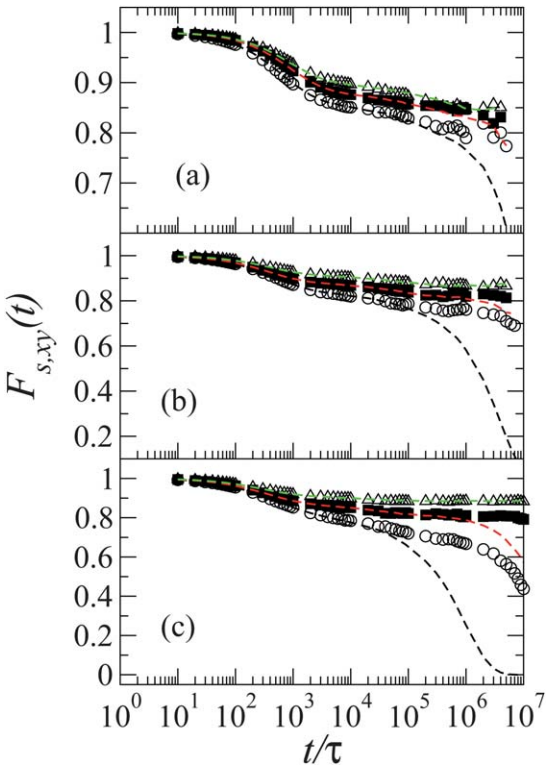

Fig. 14 Transverse self intermediate scattering functions, $F_{s,xy}(t)$, for systems of oblate hard spherocylinders with length-to-diameter ratios $L^* = 0.1$ (a), $L^* = 0.2$ (b), and $L^* = 0.3$ (c), evaluated at packing fractions $\eta = 0.575$ (circles), $\eta = 0.600$ (squares), and $\eta = 0.630$ (triangles). The black, red, and green dashed lines are Gaussian approximations (see text for details).

Additionally, we quantified the long-time structural relaxation decay by calculating the self-part of the ISFs as defined in eqn (7). In Fig. 13 and 14, we show the longitudinal, $F_{s,z}(t)$, and the transverse, $F_{s,xy}(t)$, s-ISFs at the wave vectors $q = (0,0,q_z)$ and $(q_x,q_y,0)$, respectively, corresponding to the main peaks of the static structure factor. In particular, we found that $D\sqrt{q_x^2 + q_y^2} \simeq 7$ and $Lq_z \simeq 5.0$ for the nine systems studied, with a negligible dependence on the density. We immediately notice two main features which distinguish the longitudinal and transverse structural relaxation regardless of the length-to-diameter ratio: (*i*) the in-column structural relaxation is several orders of magnitude faster than the inter-column relaxation; and (*ii*), whereas the $F_{s,z}(t)$ decays in a single step, three different time-dependent regimes are observed in the relaxation of $F_{s,xy}(t)$. More specifically, $F_{s,z}(t)$ decays very fast to zero with a slightly stretched exponential decay, as expected for dense liquidlike dynamics and already found in our previous studies on rod-like particles.[70–72] By contrast, the inter-column relaxation decay develops into two steps separated by a plateau, which denotes the average life-time of the caging effect. During the short-time decay, which is quite fast, the particles are free to rattle around their original positions inside a temporary cage composed by surrounding particles. At this stage, $F_{s,xy}(t)$ decays exponentially towards the plateau whose

height and temporal extension increase with increasing packing of the system and/or particle anisotropy. At longer time scales, a second decay, which is correlated to the escape from the transient cages, should lead the systems to the structural relaxation. However, due to the significantly long time scales and high densities involved, we are not able to quantify the long-time relaxation decay, which takes more than 7 time decades. For comparison, we also plot the Gaussian approximation $F^{G}_{s,xy}(t) = \exp\left[-\sqrt{q_x^2 + q_y^2}\cdot\left\langle \Delta x^2(t) + \Delta y^2(t)\right\rangle\right]$, which fits very well the s-ISFs at short time scales, but may substantially underestimate the time-extension of the plateau and the second decay of the structural relaxation. This result is particularly evident in the system containing particles with $L^* = 0.3$ at $\eta = 0.575$ (Fig. 14(c)), where the Gaussian fit would predict the complete structural relaxation in the time interval $10^6 < t^* < 10^7$, whereas our full calculations show a longer time scale for the relaxation to take place.

4. Conclusions

In summary, we performed the first Monte Carlo simulations of the long-time relaxation dynamics of oblate hard spherocylinders in columnar liquid crystal phases. These model systems represent a valuable reference to understand the behavior of discotic particles on molecular or colloidal scale. The structural order of the columnar mesophase has been studied by computing pair-correlation functions, which, at high pressures, indicate the formation of long-range longitudinal spatial correlations. The transverse order is hexagonal with a very weak dependence on particle anisotropy and packing of the systems. The short and long-range effect of, respectively, temporary cages and permanent barriers make the column-to-column diffusion rather slow or, at high densities, even completely inhibited. While the caging is due to the mutual trapping action of neighboring particles, the presence of the permanent barriers is associated with the crystal-like arrangement of the 2D hexagonal lattice in the direction perpendicular to the nematic director. We estimate the average life-time of the trapping cages, which extends at least for two time decades, and the height of the permanent barriers, characterized by a mean-field periodic potential. In analogy with previous studies on columnar and smectic liquid crystals of calamitic particles, the height of these barriers increases with density and/or with particle anisotropy. More specifically, the higher the barrier, the more discretized the transverse diffusion of the particles which are essentially not allowed to occupy inter-column positions. We find significantly demanding barriers, with peaks over $25k_BT$, at the highest packing fractions and anisotropies, which practically prevent the inter-column diffusion and constrain the particles to rattle around their position in the plane. By contrast, less dense systems with higher length-to-diameter ratios show more favorable free-energy landscapes with barriers in the order of a few k_BT.

While the in-column diffusion is that typical of a dense liquid with a relatively fast exponential relaxation decay, the rattling-and-jumping dynamics from column to column evolves along three separate time regimes. At very short times, the discotic particles freely diffuse in the cage formed by their nearest neighbors. At this stage, the system shows a Gaussian behavior with a linear mean square displacement and a fast exponential decay of the correlation functions. As soon as the particles feel the presence of their surrounding cage, the diffusion slows down significantly, deviations from Gaussianity are observed, and both mean square displacement and intermediate scattering function develop a plateau whose time extension increases with density and/or particle anisotropy. As time passes, an increasing number of particles jumps from a column to another, hence contributing to recover a homogeneous dynamics which results into a second diffusive regime. At the beginning of the long-time diffusion, which indicates the end of the cage regime, the deviations from Gaussian behavior start to decrease and go exponentially to zero. At high densities, the plateau may extend beyond our simulation time and no significant diffusion over the trapping cages is observed.

Finally, we have shown that the column-to-column diffusion can be strongly inhibited at high packing fractions. We believe that this result is of key importance for those applications where the hopping-type dynamics of the platelets might be unfavorable for the longitudinal charge transport through columns. Furthermore, the relatively fast dynamics along the director, especially in the proximity of the nematic or isotropic phase transition, may contribute to speed up the self-healing of structural defects, which may strongly limit the performance of columnar liquid crystals as semiconductors in a variety of devices.

Acknowledgements

We thank A. Cuetos for providing the algorithm for the computation of the distance between OHSCs, M. Marechal for providing the equilibrium data for the phase diagram of OHSCs shown in Fig. 2, and D. El Masri for fruitful discussions. This work is financed by a NWO-VICI grant and is part of the research program of the "Stichting door Fundamenteel Onderzoek der Materie (FOM)", which is financially supported by the "Nederlandse organisatie voor Wetenschappelijk Onderzoek (NWO)".

References

1 D. Vorländer, *Z. Phys. Chem., Stoechiom. Verwandtschaftsl.*, 1923, **105**, 211–254.
2 A. Isihara, *J. Chem. Phys.*, 1951, **19**, 1142–1145.
3 L. K. Runnels and C. Colvin in *Advances in Liquid Crystals*, Vol. 3 (ed.: G. H. Brown, M. M. Labes), Gordon und Breach, New York, 1972.
4 R. Alben, *Phys. Rev. Lett.*, 1973, **30**, 778–781.
5 J. P. Straley, *Phys. Rev. A: At., Mol., Opt. Phys.*, 1974, **10**, 1881–1887.
6 J. D. Brooks and G. H. Taylor, *Carbon*, 1965, **3**, 185–193.
7 S. Chandrasekhar, B. K. Sadashiva and K. A. Suresh, *Pramana*, 1977, **9**, 471–480.
8 J. Billard, J. C. Dubois, H. T. Nguyen and A. Zann, *Nouv. J. Chim.*, 1978, **2**, 535–540.
9 C. Destrade, H. T. Nguyen, H. Gasparoux, J. Malthête and A. M. Levelut, *Mol. Cryst. Liq. Cryst.*, 1981, **71**, 111–135.
10 A. M. Levelut, *J. Chem. Phys.*, 1983, **80**, 149–152.
11 S. Chandrasekhar and G. S. Ranganath, *Rep. Prog. Phys.*, 1990, **53**, 57–84.
12 S. Chandrasekhar, *Liq. Cryst.*, 1993, **14**, 3–14.
13 T. Ishi-i, T. Hirayama, K. Murakami, H. Tashiro, T. Thiemann, K. Kubo, A. Mori, S. Yamasaki, T. Akao, A. Tsuboyama, T. Mukaide, K. Ueno and S. Mataka, *Langmuir*, 2005, **21**, 1261–1268.
14 I. Paraschiv, M. Giesbers, B. van Lagen, F. C. Grozema, R. D. Abellon, L. D. A. Siebbeles, A. T. M. Marcelis, H. Zuilhof and E. J. R. Sudhölter, *Chem. Mater.*, 2006, **18**, 968–974.

15 J. Miao and L. Zhu, *Soft Matter*, 2010, **6**, 2072–2079.
16 J. D. Brand, C. Kübel, S. Ito and K. Müllen, *Chem. Mater.*, 2000, **12**, 1638–1647.
17 S. Kumar, *Liq. Cryst.*, 2004, **31**, 1037–1059.
18 M. Müller, C. Kübel and K. Müllen, *Chem.–Eur. J.*, 1998, **4**, 2099–2109.
19 R. J. Bushby and O. R. Lozman, *Curr. Opin. Colloid Interface Sci.*, 2002, **7**, 343–354.
20 W. Pisula, X. Feng and K. Müllen, *Adv. Mater.*, 2010, **22**, 3634–3649.
21 A. M. van de Craats, J. M. Warman, A. Fechtenköotter, J. D. Brand, M. A. Harbison and K. Müllen, *Adv. Mater.*, 1999, **11**, 1469–1471.
22 C. D. Simpson, J. Wu, M. D. Watson and K. Müllen, *J. Mater. Chem.*, 2004, **14**, 494–504.
23 I. O. Shklyarevskiy, P. Jonkheijm, N. Stutzmann, D. Wasserberg, H. J. Wondergem, P. C. M. Christianen, A. P. H. J. Schenning, D. M. de Leeuw, Z. Tomovic, J. Wu, K. Müllen and J. C. Maan, *J. Am. Chem. Soc.*, 2005, **127**, 16233–16237.
24 J. Piris, M. G. Debije, N. Stutzmann, B. W. Laursen, W. Pisula, M. D. Watson, T. Bjornholm, K. Müllen and J. M. Warman, *Adv. Funct. Mater.*, 2004, **14**, 1053–1061.
25 P. G. Schouten, J. M. Warman, G. H. Gelinck and M. J. Copyn, *J. Phys. Chem.*, 1995, **99**, 11780.
26 J. M. Warman, J. Piris, W. Pisula, M. Kastler, D. Wasserfallen and K. Müllen, *J. Am. Chem. Soc.*, 2005, **127**, 14257–14261.
27 H. Iino, J. Hanna, R. J. Bushby, B. Movaghar, B. J. Whitaker and M. J. Cook, *Appl. Phys. Lett.*, 2005, **87**, 132102.
28 J. H. Burroughes, D. D. C. Bradley, A. R. Brown, R. N. Marks, K. Mackay, R. H. Friend, P. L. Burns and A. B. Holmes, *Nature*, 1990, **347**, 539–541.
29 G. Yu, J. Gao, J. C. Hummelen, F. Wudl and A. J. Heeger, *Science*, 1995, **270**, 1789–1791.
30 J. J. M. Halls, C. A. Walsh, N. C. Greenham, E. A. Marseglia, R. H. Friend, S. C. Moratti and A. B. Holmes, *Nature*, 1995, **376**, 498–500.
31 T. Christ, V. Stumpflen and J. H. Wendorff, *Macromol. Rapid Commun.*, 1997, **18**, 93–98.
32 A. Kraft, A. C. Grimsdale and A. B. Holmes, *Angew. Chem., Int. Ed.*, 1998, **37**, 402–428.
33 S. Furumi, D. Janietz, M. Kidowaki, M. Nakagawa, S. Morino, J. Stumpe and K. Ichimura, *Chem. Mater.*, 2001, **13**, 1434–1437.
34 L. Schmidt-Mende, A. Fechtenkötter, K. Müllen, E. Moons, R. H. Friend and J. D. MacKenzie, *Science*, 2001, **293**, 1119–1122.
35 J. P. Schmidtke, R. H. Friend, M. Kastler and K. Müllen, *J. Chem. Phys.*, 2006, **124**, 174704.
36 N. Boden, R. J. Bushby, J. Clements, B. Movaghar, K. J. Donovan and T. Kreouzis, *Phys. Rev. B: Condens. Matter*, 1995, **52**, 13274–13280.
37 M. C. D. Mourad, E. Groeneveld, P. J. de Lange, C. Vonk, D. van der Beekb and H. N. W. Lekkerkerker, *J. Mater. Chem.*, 2008, **18**, 3004–3010.
38 C. T. Kresge, M. E. Leonowicz, W. J. Roth, J. C. Vartuli and J. S. Beck, *Nature*, 1992, **359**, 710–712.
39 G. S. Attard, J. C. Glyde and C. G. Göltner, *Nature*, 1995, **378**, 366–368.
40 M. C. D. Mourad, D. V. Byelov, A. V. Petukhov, D. A. M. de Winter, A. J. Verkleij and H. N. W. Lekkerkerker, *J. Phys. Chem. B*, 2009, **113**, 11604–11613.
41 F. M. van der Kooij, K. Kassapidou and H. N. W. Lekkerkerker, *Nature*, 2000, **406**, 868–871.
42 A. A. Verhoeff, R. H. J. Otten, P. van der Schoot and H. N. W. Lekkerkerker, *J. Phys. Chem. B*, 2009, **113**, 3704–3708.
43 M. Kroon, W. L. Vos and G. H. Wegdam, *Phys. Rev. E: Stat. Phys., Plasmas, Fluids, Relat. Interdiscip. Top.*, 1998, **57**, 1962–1970.
44 D. Bonn, H. Kellay, H. Tanaka, G. Wegdam and J. Meunier, *Langmuir*, 1999, **15**, 7534–7536.
45 P. Mongondry, J. F. Tassin and T. Nicolai, *J. Colloid Interface Sci.*, 2005, **283**, 397–405.
46 B. Ruzicka, L. Zulian and G. Ruocco, *Langmuir*, 2006, **22**, 1106–1111.
47 B. Ruzicka, L. Zulian, E. Zaccarelli, R. Angelini, M. Sztucki, A. Moussaïd and G. Ruocco, *Phys. Rev. Lett.*, 2010, **104**, 085701.
48 D. Frenkel and R. Eppenga, *Phys. Rev. Lett.*, 1982, **49**, 1089–1092.
49 M. A. Bates and D. Frenkel, *Phys. Rev. E: Stat. Phys., Plasmas, Fluids, Relat. Interdiscip. Top.*, 1998, **57**, 4824–4826.
50 L. Harnau and S. Dietrich, *Phys. Rev. E: Stat. Phys., Plasmas, Fluids, Relat. Interdiscip. Top.*, 2002, **65**, 021505.
51 M. Bier, L. Harnau and S. Dietrich, *Phys. Rev. E: Stat., Nonlinear, Soft Matter Phys.*, 2004, **69**, 021506.
52 M. Bier, L. Harnau and S. Dietrich, *J. Chem. Phys.*, 2005, **123**, 114906.
53 M. Bier, L. Harnau and S. Dietrich, *J. Chem. Phys.*, 2006, **125**, 184704.
54 D. van der Beek, H. Reich, P. van der Schoot, M. Dijkstra, T. Schilling, R. Vink, M. Schmidt, R. van Roij and H. Lekkerkerker, *Phys. Rev. Lett.*, 2006, **97**, 087801.
55 H. Reich, M. Dijkstra, R. van Roij and M. Schmidt, *J. Phys. Chem. B*, 2007, **111**, 7825–7835.
56 K. Zhao, C. Harrison, D. Huse, W. B. Russel and P. M. Chaikin, *Phys. Rev. E: Stat., Nonlinear, Soft Matter Phys.*, 2007, **76**, 040401.
57 D. L. Cheung, L. Anton, M. P. Allen, A. J. Masters, J. Phillips and M. Schmidt, *Phys. Rev. E: Stat., Nonlinear, Soft Matter Phys.*, 2008, **78**, 041201.
58 J. Phillips and M. Schmidt, *Phys. Rev. E: Stat., Nonlinear, Soft Matter Phys.*, 2010, **81**, 041401.
59 I. Ono and S. Kondo, *Bull. Chem. Soc. Jpn.*, 1992, **65**, 1057–1061.
60 A. Maliniak, *J. Chem. Phys.*, 1992, **96**, 2306–2317.
61 G. Cinacchi, R. Colle and A. Tani, *J. Phys. Chem. B*, 2004, **108**, 7969–7977.
62 D. Andrienko, V. Marcon and K. Kremer, *J. Chem. Phys.*, 2006, **125**, 124902.
63 P. L. Cristinziano and F. Lelj, *J. Chem. Phys.*, 2007, **127**, 134506.
64 G. Voth, *J. Chem. Theory Comput.*, 2006, **2**, 463.
65 S. C. McGrother, D. C. Williamson and G. Jackson, *J. Chem. Phys.*, 1996, **104**, 6755–6771.
66 P. Bolhuis and D. Frenkel, *J. Chem. Phys.*, 1997, **106**, 666–687.
67 E. de Miguel, E. Martín del Río and F. J. Blas, *J. Chem. Phys.*, 2004, **121**, 11183.
68 B. Martínez-Haya, A. Cuetos, S. Lago and L. F. Rull, *J. Chem. Phys.*, 2005, **122**, 024908.
69 A. Patti, D. El Masri, R. van Roij and M. Dijkstra, *Phys. Rev. Lett.*, 2009, **103**, 248304.
70 A. Patti, D. El Masri, R. van Roij and M. Dijkstra, *J. Chem. Phys.*, 2010, **132**, 224907.
71 R. Matena, M. Dijkstra and A. Patti, *Phys. Rev. E*, 2010, **81**, 021704.
72 S. Belli, A. Patti, R. van Roij and M. Dijkstra, *J. Chem. Phys.*, 2010, **133**, 154514.
73 A. Cuetos and B. Martínez-Haya, *J. Chem. Phys.*, 2008, **129**, 214706.
74 B. Martínez-Haya and A. Cuetos, *J. Chem. Phys.*, 2009, **131**, 074901.
75 B. Martínez-Haya and A. Cuetos, *Mol. Simul.*, 2009, **35**, 1077–1083.
76 D. Frenkel, B. M. Mulder and J. P. McTague, *Phys. Rev. Lett.*, 1984, **52**, 287–290.
77 M. A. Bates and G. R. Luckhurst, *J. Chem. Phys.*, 1996, **104**, 6696–6709.
78 J. A. C. Veerman and D. Frenkel, *Phys. Rev. A: At., Mol., Opt. Phys.*, 1992, **45**, 5632–5648.
79 M. Marechal, *Anistropic Colloids: Bulk Phase Behavior and Equilibrium Sedimentation*, Ph.D. Thesis, Utrecht University, the Netherlands, 2009, ISBN: 978-90-393-5166-6.
80 L. Filion, M. Marechal, B. van Oorschot, D. Pelt, F. Smallenburg and M. Dijkstra, *Phys. Rev. Lett.*, 2009, **103**, 188302.
81 T. Gleim, W. Kob and K. Binder, *Phys. Rev. Lett.*, 1998, **81**, 4404–4407.
82 G. Szamel and E. Flenner, *Europhys. Lett.*, 2004, **67**, 779–785.
83 F. Höfling, T. Munk, E. Frey and T. Franosch, *J. Chem. Phys.*, 2008, **128**, 164517.
84 M. Bier and R. van Roij, *Phys. Rev. E: Stat., Nonlinear, Soft Matter Phys.*, 2007, **76**, 021405.
85 P. M. Richards, *Phys. Rev. B: Solid State*, 1977, **16**, 1393.
86 M. Wojcik and K. E. Gubbins, *Mol. Phys.*, 1984, **53**, 397.
87 P. D. Duncan, M. Dennison, A. J. Masters and M. R. Wilson, *Phys. Rev. E: Stat., Nonlinear, Soft Matter Phys.*, 2009, **79**, 031702.
88 A. Neff, *IBM J. Res. Dev.*, 1990, **34**, 770.
89 H. A. Almohamad and S. Z. Selim, *Appl. Math. Modell.*, 2003, **27**, 115.
90 V. Pryamitsyn and V. Ganesan, *J. Chem. Phys.*, 2008, **128**, 134901.
91 L. Berthier and W. Kob, *J. Phys.: Condens. Matter*, 2007, **19**, 205130.
92 L. Pfleiderer, K. Milinkovic and T. Schilling, *Europhys. Lett.*, 2008, **84**, 16003.
93 F. Perrin, *J. Phys. Radium*, 1936, **7**, 1.

94 H. Shimizu, *J. Chem. Phys.*, 1962, **37**, 765.
95 G. Odriozola, M. Romero-Bastida and F. de J. Guevara-Rodríguez, *Phys. Rev. E: Stat., Nonlinear, Soft Matter Phys.*, 2004, **70**, 021405.
96 M. P. Lettinga and E. Grelet, *Phys. Rev. Lett.*, 2007, **99**, 197802.
97 L. Van Hove, *Phys. Rev.*, 1954, **95**, 249.
98 A. Rahman, *Phys. Rev.*, 1964, **136**, A405.
99 M. Bier, R. van Roij, M. Dijkstra and P. van der Schoot, *Phys. Rev. Lett.*, 2008, **101**, 215901.
100 D. Frenkel and B. Smit, *Understanding Molecular Simulation: From Algorithms to Applications*, Academic Press, 2 nd Ed., 2002.